

Correlation effects in Ni 3d states of LaNiPO

A. V. Lukoyanov,^{1,2} S. L. Skornyakov,^{1,2} J. A. McLeod,³ M. Abu-Samak,⁴ R. G. Wilks,³ E. Z. Kurmaev,¹

A. Moewes,³ N. A. Skorikov,¹ Yu. A. Izyumov,¹ L. D. Finkelstein,¹ V. I. Anisimov,¹ and D. Johrendt⁵

¹*Institute of Metal Physics, Russian Academy of Sciences–Ural Division, 620990 Yekaterinburg, Russia*

²*Ural State Technical University–UPI, 620002 Yekaterinburg, Russia*

³*Department of Physics and Engineering Physics,*

University of Saskatchewan, 116 Science Place, S7N 5E2 Saskatoon, Canada

⁴*Physics Department, Al-Hussein Bin Talal University, P.O. Box 20, Ma'an, Jordan*

⁵*Department Chemie und Biochemie der Ludwig-Maximilians-Universität München, Butenandtstrasse 5-13 (Haus D), 81377 München, Germany*

(Dated: October 30, 2018)

The electronic structure of the new superconducting material LaNiPO experimentally probed by soft X-ray spectroscopy and theoretically calculated by the combination of local density approximation with Dynamical Mean-Field Theory (LDA+DMFT) are compared herein. We have measured the Ni $L_{2,3}$ X-ray emission (XES) and absorption (XAS) spectra which probe the occupied and unoccupied the Ni 3d states, respectively. In LaNiPO, the Ni 3d states are strongly renormalized by dynamical correlations and shifted about 1.5 eV lower in the valence band than the corresponding Fe 3d states in LaFeAsO. We further obtain a lower Hubbard band at -9 eV below the Fermi level in LaNiPO which bears striking resemblance to the lower Hubbard band in the correlated oxide NiO, while no such band is observed in LaFeAsO. These results are also supported by the intensity ratio between the transition metal L_2 and L_3 bands measured experimentally to be higher in LaNiPO than in LaFeAsO, indicating the presence of the stronger electron correlations in the Ni 3d states in LaNiPO in comparison with the Fe 3d states in LaFeAsO. These findings are in accordance with resonantly excited transition metal L_3 X-ray emission spectra which probe occupied metal 3d-states and show the appearance of the lower Hubbard band in LaNiPO and NiO and its absence in LaFeAsO.

PACS numbers: 71.27.+a, 74.25.Jb, 78.70.En

I. INTRODUCTION

The superconductivity of the quaternary transition metal oxyphosphides LaFePO ($T_c = 3.2$ K) and LaNiPO ($T_c = 3.0 - 4.3$ K) was discovered recently¹⁻³ although these compounds have been under study for more than ten years.⁴ In spite of the relatively low superconducting transition temperatures T_c , these materials are important because they triggered the extensive search for superconductivity in oxyarsenides $LnMeAsO$ (where $Ln = La, Ce, Pr, Nd, Sm, Gd$; $Me = 3d$ metals). This search has proven to be remarkably successful, reaching T_c s of up to 55 K⁵⁻¹⁰ and strong upper critical fields H_{c2} of up to 100 T.¹¹

Despite the focus on oxyarsenides, Ni and Fe oxyphosphides still attract attention¹²⁻¹⁶ because while they share the same bi-layer structure as $LnMeAsO$ materials, the mechanism for superconductivity appears to be different. In particular the value of the total electron-phonon coupling constant λ in LaFeAsO is much lower than in conventional electron-phonon coupling superconductors, for example, compare the $\lambda = 0.21$ of LaFeAsO¹⁷ with the $\lambda = 0.44$ of Al (where $T_c = 1.3$ K for Al), and even the inclusion of multiband effects fails to explain the observed T_c of 26 K.¹⁸ For LaNiPO the coupling constant is more than two times higher ($\lambda = 0.58$) and the superconducting properties can be described within the Migdal-Eliashberg theory.¹⁸ Herein we interpret soft X-ray emission and absorption spectra of LaNiPO and

LaFeAsO¹⁹ and compare the measurements with our local density approximation with Dynamical Mean Field Theory (LDA+DMFT) electronic structure calculations to investigate the similarities and differences between these two types of superconductors. To assist in investigating these materials, electronic structure calculations of LaFePO²⁰ ($T_c = 3.2$ K¹) and NiO²¹ were used.

LaFeAsO, unlike LaNiPO and LaFePO, is not superconducting unless doping^{22,23} or high pressure^{24,25} is applied to suppress the magnetic transition temperature.²⁵ Since these materials share the same basic ambient crystal structure and atomic constituents, yet exhibit different low-temperature properties, a basic study of the ambient electronic structure of these three materials is of interest, especially since the bulk electronic structure of these materials is insensitive to temperature or magnetic phase changes.²⁶

II. EXPERIMENTAL AND CALCULATION DETAILS

Single crystals of LaNiPO were synthesized by heating a mixture of 375.0 mg La (99.9%, Smart Elements), 201.7 mg NiO (99.99%, Sigma-Aldrich) and 83.6 mg P (red, 99%, Sigma-Aldrich) with 2000 mg Sn (99.99%, Alfa Aesar) in an alumina crucible, which was sealed in a silica tube under an atmosphere of purified argon. The sample was heated to 1173 K at a rate of 40 K/h,

kept at this temperature for 10 days and slowly cooled down to room temperature at a rate of 3 K/h. The crucible was smashed and the tin bar dissolved in 6 M HCl at room temperature. The remaining sample consisted of single crystals of LaNiPO beside small amounts of LaNi₂P₂ (7%), Ni₂SnP (4%) and Ni₃Sn₄ (< 1%). Further attempts to optimize the synthesis conditions with regard to reaction temperature or duration were unsuccessful. Samples prepared directly from the starting material without tin flux yielded only small amounts of LaNiPO with LaNi₂P₂ as the main product. For details of preparation see Ref. 3. The soft X-ray absorption and emission measurements of the metal $L_{2,3}$ edges were performed at the soft X-ray fluorescence endstation of Beamline 8.0.1 at the Advanced Light Source in the Lawrence Berkeley National Laboratory.²⁷ The endstation uses a Rowland circle geometry X-ray spectrometer with spherical gratings and an area-sensitive multichannel detector. We measured the resonant and non-resonant Ni $L_{2,3}$ ($3d, 4s \rightarrow 2p$ transition) X-ray emission spectra (XES) for LaNiPO. Additional non-resonant XES measurements of the Ni $L_{2,3}$ edges of Ni metal foil and NiO were obtained as reference standard. The instrumental resolving power ($E/\Delta E$) for emission measurements was about 10^3 . The X-ray absorption spectra (XAS) were measured in total electron yield (TEY) mode for the Ni $L_{2,3}$ edges. The instrumental resolving power ($E/\Delta E$) for absorption measurements was about 5×10^3 . All absorption spectra were normalized to the incident photon current using a highly transparent gold mesh in front of the sample to correct for intensity fluctuations in the incoming photon beam. The excitation energies for the Ni $L_{2,3}$ resonant X-ray emission spectra were determined from the XAS spectra and the energies were selected at the L_3 and L_2 thresholds.

Electronic structure calculations were performed within the pseudopotential plane-wave method PWSCF, as implemented in the Quantum ESPRESSO package.²⁸ We used the generalized gradient approximation in the Perdew-Burke-Ernzerhof version²⁹ for the exchange-correlation potential in the Rappe-Rabe-Kaxiras-Joannopoulos form.³⁰ The Brillouin zone integration was performed with a $15 \times 15 \times 15$ k-point grid. A kinetic-energy cutoff of 45 Ry was employed for the plane-wave expansion of the electronic states. The experimentally determined lattice parameters and internal atom positions of LaNiPO ($a = 4.0461 \text{ \AA}$, $c = 8.100 \text{ \AA}$)² were used.

To include dynamical correlation effects in the $3d$ shell of Ni, we performed the LDA+DMFT³¹ calculations for LaNiPO. Following the Wannier function projection procedure of Ref. 32, we constructed an effective H_{LDA} Hamiltonian and then used it to solve the Dynamical Mean-Field Theory (DMFT)³³ self-consistency equations. The H_{LDA} Hamiltonian contained 22 bands due to five Ni $3d$, three O $2p$, and three P $3p$ orbitals per formula unit, projected in a single energy window that explicitly takes into account the hybridization between p

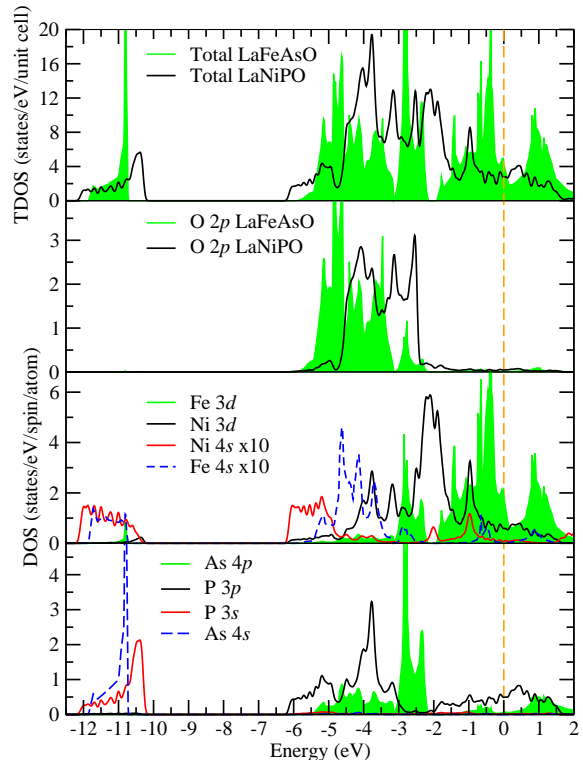


FIG. 1: (Color online) Total and partial densities of states for LaNiPO (in comparison with LaFeAsO from Ref. 36) obtained within the density functional theory (DFT) calculations. The dashed lines in the Ni, Fe $4s$, $3d$ DOS refer to the metal $4s$ states magnified by a factor of 10. La does not have any significant contribution to the valence band, and is not shown here.

and d electrons.³²

The DMFT auxiliary impurity problem was solved by the hybridization function expansion Continuous-Time Quantum Monte-Carlo method.³⁴ The elements of Coulomb interaction matrix were parameterized by U and J parameters.³⁵ We used interaction parameters $U = 8 \text{ eV}$ and $J = 1 \text{ eV}$ for LaNiPO similar to the values obtained in Ref. 21. Calculations were performed in the paramagnetic state at the inverse temperature $\beta = 1/T = 20 \text{ eV}^{-1}$. The real-axis self-energy needed to calculate spectral functions was obtained by the Padé approximant.³⁷

III. RESULTS AND DISCUSSION

The calculated noncorrelated electronic structure of LaNiPO is shown in Fig. 1 in comparison with the structure of LaFeAsO.³⁶ These calculations are in agreement with other DOS calculations available to date.^{12,13} In all cases the far bottom of the valence band (-11 eV) consists of P $3s$ or As $4s$. The top of the valence band (-2 eV to 0 eV) consists almost solely of metal $3d$ states in both cases. Between -2 and -4 eV there is strong

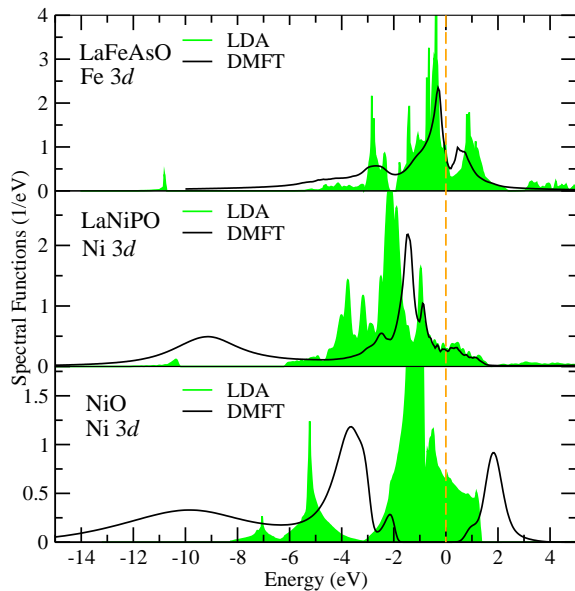


FIG. 2: (Color online) Densities of states for Ni 3d and Fe 3d orbitals obtained within DFT (filled areas) and the LDA+DMFT total 3d spectral functions (solid lines). Data for LaFeAsO³⁶ and NiO²¹ are given for comparison.

hybridization between the O 2p and Ni 3d states in LaNiPO; in LaFeAsO there are far fewer Fe 3d states in this region indicating much weaker hybridization. The situation is the same with LaFePO.²⁰ LaNiPO also has a reduction in metal 3d states and total states at the Fermi level compared to LaFeAsO and LaFePO. This may explain why Ni-based superconductors have lower T_c values than FeAs-based superconductors. For all compounds the P 3s, 3p and As 4s, 4p states, respectively, occupy the same basic region in the valence band and do not contribute significantly to the Fermi level. The La 5p states are identical for both compounds, they have atomic-like character and do not contribute to the valence band; they are not shown here.

The spectral function from the LDA+DMFT calculation for the Ni 3d states of LaNiPO is shown in Fig. 2 (middle panel). In the energy interval from -1 to 1 eV near the Fermi energy the 3d spectral function is close to the noncorrelated LDA density of states. However, below these energies the spectral function is substantially renormalized with the formation of a strong peak at -1.5 eV, and the appearance of a lower Hubbard band: the broad peak centered at -9.1 eV. Thus this picture resembles the LDA+DMFT results for LaFeAsO³⁶ (upper panel) only for the energies above -6 eV, since in LaFeAsO the lower Hubbard band was not found. In NiO, however, a similar broad peak centered at -10 eV is obtained, as shown in the lower panel of Fig. 2. This lower Hubbard band is evidence for strong correlations,²¹ and this is a clear indication of strong correlations in LaNiPO, similar to NiO.³⁸ The comparison of the LDA+DMFT calculation for Ni 3d states of LaNiPO and NiO and Fe 3d states

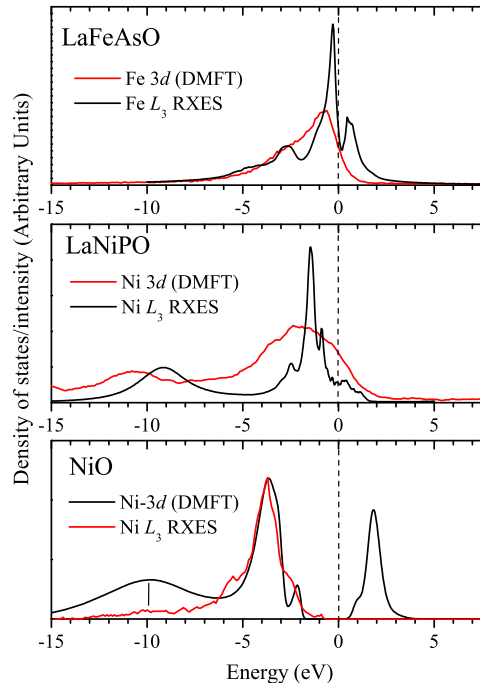


FIG. 3: (Color online) Comparison of the LDA+DMFT total 3d spectral functions (LaFeAsO from Ref. 36 and NiO from Ref. 21) with the resonantly excited Ni L_3 and Fe L_3 X-ray emission spectra.

of LaFeAsO with the resonantly excited Ni L_3 and Fe L_3 X-ray emission spectra which probe occupied Me 3d states is presented in Fig. 3. The occurrence of the lower Hubbard band in LaNiPO and NiO and its absence in LaFeAsO is confirmed by experimental XES spectra.

The soft X-ray metal (Ni, Fe) $L_{2,3}$ spectra are shown in Fig. 4. The metal $L_{2,3}$ XES indicate two main bands separated by the spin-orbit splitting of the metal 2p states. The lower intensity high energy band corresponds to the L_2 emission line ($3d,4s \rightarrow 2p_{1/2}$ transitions), and the higher intensity low energy band corresponds to the L_3 emission line ($3d,4s \rightarrow 2p_{3/2}$ transitions). The resonant L_2 and L_3 XES (curves b and c in the bottom panels, respectively) have the same basic shape. The lack of resonant features indicates that the spectra primarily measuring the partial occupied DOS rather than multiplet or inelastic scattering effects. Note that the La $M_{4,5}$ XES appears below the Ni L_3 emission line in the resonant Ni L_3 spectrum. The metal $L_{2,3}$ XAS are presented in the top panels of Fig. 4. According to dipole selection rules ($\Delta l = \pm 1$) they correspond to the excitation of metal 2p-core level electrons into unoccupied 3d states. Unfortunately these spectra can not probe the unoccupied 3d DOS directly because the core-hole causes an increased effective nuclear charge distorting the local DOS levels. Further, simulating $L_{2,3}$ XAS requires consider-

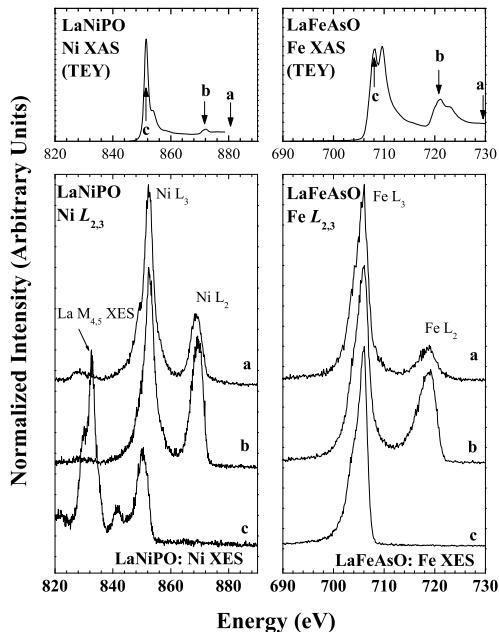


FIG. 4: Summary of spectra for LaNiPO (left panel) and LaFeAsO (right panel). The upper panels show the metal $L_{2,3}$ XAS (in TEY mode), the lower panels the resonant and non-resonant metal $L_{2,3}$ XES. The excitation energies are indicated by arrows in the XAS plots.

ing multiplet splitting, hybridization, and crystal field effects. One such simulation was recently conducted for LaFeAsO in Ref. 39, to our knowledge no similar simulation of LaNiPO exists. Therefore we include the metal $L_{2,3}$ XAS only for completeness. Resonantly excited Ni L_3 XES of LaNiPO (curve c) shows the presence of La $M_{4,5}$ XES because excitation energy in this case is very close to resonant excitation of La M -emission spectra.

The ratio of the integral-intensity of the metal L_2 and L_3 peaks (the $I(L_2)/I(L_3)$ ratio) for LaFeAsO is roughly the same as that of metallic Fe, and quite different from that of strongly correlated FeO (see Fig. 5, right side, bottom panel). In a free atom, the $I(L_2)/I(L_3)$ ratio should be equal to 1/2 as the ratio is based solely on the statistical population of the $2p_{1/2}$ and $2p_{3/2}$ levels. In metals the radiationless $L_2L_3M_{4,5}$ Coster-Kronig (C-K) transitions greatly reduce the $I(L_2)/I(L_3)$ ratio,⁴⁰ and the $I(L_2)/I(L_3)$ ratio can be used as a measure for the electron correlation strength of a transition metal compound⁴¹ (see Fig. 5, right side, top panel). The full width at half maximum (FWHM) of the L_3 band in LaFeAsO is again closer to that of metallic Fe than FeO (see Fig. 5, right side, middle panel). While this does not directly prove anything, it suggests that the Fe $3d$ electronic structure of LaFeAsO may be similar to that of metallic Fe. The shape and statistics of the Fe $L_{2,3}$ XES indicate that the Fe $3d$ states in LaFeAsO are not

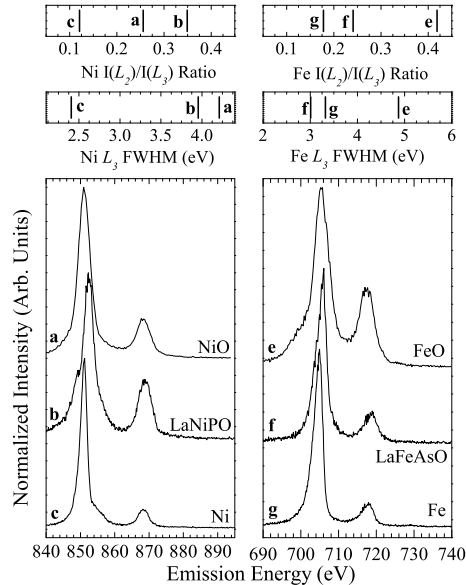


FIG. 5: Comparison of non-resonant metal $L_{2,3}$ XES of NiO, LaNiPO, and Ni (left side panels) and FeO, LaFeAsO, and Fe (right side panels) from Ref. 19. The $I(L_2)/I(L_3)$ ratios for each system are shown in the top panels, and the full width at half maximum (FWHM) of the L_3 bands are shown in the middle panels. The metal $L_{2,3}$ XES are shown in the bottom panels, for easy reference. The $I(L_2)/I(L_3)$ ratios were calculated by taking the quotient of the integrals of the L_2 and L_3 bands.

strongly correlated.

In contrast to LaFeAsO, the $I(L_2)/I(L_3)$ ratio for LaNiPO is much greater than that of Ni metal, as is the FWHM of the LaNiPO L_3 band (see Fig. 5, left side, bottom panel). Indeed, the $I(L_2)/I(L_3)$ ratio and L_3 FWHM for LaNiPO (see Fig. 5, left side, top and middle panels) are rather close to those of correlated NiO. Since the transition metal $I(L_2)/I(L_3)$ ratio is over 50% greater in LaNiPO than LaFeAsO, and since in NiO is comparable to FeO in terms of “correlation strength”,⁴² the Ni $3d$ states are more correlated than the LaFeAsO Fe $3d$ states.

IV. CONCLUSIONS

We have studied the electronic structure of LaNiPO excited by synchrotron soft X-ray emission and absorption spectroscopy and obtained the theoretical spectral functions within the combination of local density approximation with Dynamical Mean-Field Theory (LDA+DMFT). We conclude that the Ni $3d$ states of LaNiPO reside deeper in the valence band than the Fe $3d$ states of LaFeAsO. The greater occupation in the metal $3d$ bands in LaNiPO reduces the density of the states at the Fermi

level and increases the hybridization with O $2p$ states compared to those in LaFeAsO. Accounting for dynamical correlation in the Ni $3d$ states of LaNiPO results in the renormalization of the states below the Fermi energy and the formation of the lower Hubbard band centered at -9 eV, similar to NiO, but in contrast to LaFeAsO. The $I(L_2)/I(L_3)$ ratio is much higher in LaNiPO than in LaFeAsO, indicating the Ni $3d$ states of LaNiPO have stronger electron correlations than the Fe $3d$ states of LaFeAsO.

V. ACKNOWLEDGMENTS

The authors thank J. Kuneš for providing the DMFT code and P. Werner for the CT-QMC impurity solver

used in our calculations. This work was supported by the Research Council of the President of the Russian Federation (Grant NSH-4711.2010.2), the Russian Science Foundation for Basic Research (Projects 08-02-00148, 10-02-00046, and 10-02-00546), the Natural Sciences and Engineering Research Council of Canada (NSERC) and the Canada Research Chair program, Russian Federal Agency for Science and Innovations (Program “Scientific and Scientific-Pedagogical Training of the Innovating Russia” for 2009-2010 years), grant No. 02.740.11.0217, the Dynasty Foundation.

-
- ¹ Y. Kamihara, H. Hiramatsu, M. Hirano, R. Kawamura, H. Yanagi, T. Kamiya, and H. Hosono, *J. Am. Chem. Soc.* **128**, 10012 (2006).
- ² T. Watanabe, H. Yanagi, T. Kamiya, Y. Kamihara, H. Hiramatsu, M. Hirano, and H. Hosono, *Inorg. Chem.* **46**, 7719 (2007).
- ³ M. Tegel, D. Bichler, and D. Johrendt, *Solid State Sci.* **10**, 193 (2008).
- ⁴ B. I. Zimmer, W. Jeitschko, J. H. Albering, R. Glaum, and M. Reehuis, *J. Alloys Comp.* **229**, 238 (1995).
- ⁵ Y. Kamihara, T. Watanabe, M. Hirano, and H. Hosono, *J. Am. Chem. Soc.* **130**, 3296 (2008).
- ⁶ H.-H. Wen, G. Mu, L. Fang, H. Yang, and X. Zhu, *Europhys. Lett.* **82**, 17009 (2008).
- ⁷ X. H. Chen, T. Wu, G. Wu, R. H. Liu, H. Chen, and D. F. Fang, *Nature* **453**, 761 (2008).
- ⁸ Z.-A. Ren, J. Yang, W. Lu, W. Yi, G.-C. Che, X.-L. Dong, L.-L. Sun, and Z.-X. Zhao, *Materials Research Innovations* **12**, 105 (2008).
- ⁹ Z.-A. Ren, J. Yang, W. Lu, W. Yi, X.-L. Shen, Z.-C. Li, G.-C. Che, X.-L. Dong, L.-L. Sun, Z. Fand, and Z.-X. Zhao, *Europhys. Lett.* **82**, 57002 (2008).
- ¹⁰ R. H. Liu, G. Wu, T. Wu, D. F. Fang, H. Chen, S. Y. Li, K. Liu, Y. L. Xie, X. F. Wang, R. L. Yang, L. Ding, C. He, D. L. Feng, and X. H. Chen, *Phys. Rev. Lett.* **101**, 087001 (2008).
- ¹¹ C. Senatore, R. Flükiger, M. Cantoni, G. Wu, R. H. Liu, and X. H. Chen, *Phys. Rev. B* **78**, 054514 (2008).
- ¹² S. Lebègue, *Phys. Rev. B* **75**, 035110 (2007).
- ¹³ W.-B. Zhang, X.-B. Xiao, W.-Y. Yu, N. Wang, and B.-Y. Tang, *Phys. Rev. B* **77**, 214513 (2008).
- ¹⁴ C. Y. Liang, R. C. Che, H. X. Yang, H. F. Tian, R. J. Xiao, J. B. Lu, R. Li, and J. Q. Li, *Supercond. Sci. Technol.* **20**, 687 (2007).
- ¹⁵ R. Che, R. Xiao, C. Liang, H. Yang, C. Ma, H. Shi, and J. Li, *Phys. Rev. B* **77**, 184518 (2008).
- ¹⁶ Q. Si and E. Abrahams, *Phys. Rev. Lett.* **101**, 076401 (2008).
- ¹⁷ L. Boeri, O. V. Dolgov, and A. A. Golubov, *Phys. Rev. Lett.* **101**, 026403 (2008).
- ¹⁸ L. Boeri, O. V. Dolgov, and A. A. Golubov, *Physica C: Superconductivity* **469**, 628 (2009).
- ¹⁹ E. Z. Kurmaev, R. G. Wilks, A. Moewes, N. A. Skorikov, Yu. A. Izyumov, L. D. Finkelstein, R. H. Li, and X. H. Chen, *Phys. Rev. B* **78**, 220503(R) (2008).
- ²⁰ S. L. Skornyakov, N. A. Skorikov, A. V. Lukoyanov, A. O. Shorikov, and V. I. Anisimov, arXiv:condmat/1002.4947.
- ²¹ J. Kuneš, V. I. Anisimov, A. V. Lukoyanov, and D. Vollhardt, *Phys. Rev. B* **75**, 165115 (2007).
- ²² Z. Li, G. Chen, J. Dong, G. Li, W. Hu, D. Wu, S. Su, P. Zheng, T. Xiang, N. Wang, and J. Luo, *Phys. Rev. B* **78**, 060504(R) (2008).
- ²³ J. Dong, H. J. Zhang, G. Xu, Z. Li, G. Li, W. Z. Hu, D. Wu, G. F. Chen, X. Dai, J. L. Luo, Z. Fang, and N. L. Wang, *Europ. Phys. Lett.* **83**, 27006 (2008).
- ²⁴ Y. Yang and X. Hu, *J. Appl. Phys.* **106**, 073910 (2009).
- ²⁵ C. W. Chu and B. Lorenz, *Physica C: Superconductivity* **469**, 385 (2009).
- ²⁶ T. Yildirim, *Phys. Rev. Lett.* **102**, 037003 (2009).
- ²⁷ J. J. Jia, T. A. Callcott, J. Yurkas, A. W. Ellis, F. J. Himpsel, M. G. Samant, J. Stöhr, D. L. Ederer, J. A. Carlisle, E. A. Hudson, L. J. Terminello, D. K. Shuh, and R. C. C. Perera, *Rev. Sci. Instrum.* **66**, 1394 (1995).
- ²⁸ P. Giannozzi *et al.*, *J. Phys.: Condens. Matter* **21**, 395502 (2009).
- ²⁹ J. P. Perdew, K. Burke, and M. Ernzerhof, *Phys. Rev. Lett.* **77**, 3865 (1996).
- ³⁰ A. M. Rappe, K. M. Rabe, E. Kaxiras, and J. D. Joannopoulos, *Phys. Rev. B* **41**, 1227 (1990).
- ³¹ K. Held, I. A. Nekrasov, G. Keller, V. Eyert, N. Blümer, A. K. McMahan, R. T. Scalettar, Th. Pruschke, V. I. Anisimov, and D. Vollhardt, *Phys. Stat. Sol. (b)* **243**, 2599 (2006).
- ³² Dm. M. Korotin, A. V. Kozhevnikov, S. L. Skornyakov, I. Leonov, N. Binggeli, V. I. Anisimov, and G. Trimarchi, *Europ. Phys. J. B* **65**, 91 (2008).
- ³³ A. Georges, G. Kotliar, W. Krauth, and M. J. Rozenberg, *Rev. Mod. Phys.* **68**, 13 (1996).
- ³⁴ P. Werner, E. Gull, A. Comanac, L. de Medici, M. Troyer, and A. J. Millis, *Phys. Rev. Lett.* **97**, 076405 (2006).
- ³⁵ A. I. Liechtenstein, V. I. Anisimov, and J. Zaanen, *Phys. Rev. B* **52**, R5467 (1995).
- ³⁶ V. I. Anisimov, Dm. M. Korotin, M. A. Korotin,

- A. V. Kozhevnikov, J. Kuneš, A. O. Shorikov, S. L. Skornyakov, and S. V. Streltsov, *J. Phys.: Condens. Matter* **21**, 075602 (2009).
- ³⁷ H. J. Vidberg and J. W. Serene, *J. Low Temp. Phys.* **29**, 179 (1977).
- ³⁸ E. Z. Kurmaev, R. G. Wilks, A. Moewes, L. D. Finkelstein, S. N. Shamin, and J. Kuneš, *Phys. Rev. B* **77**, 165127 (2008).
- ³⁹ T. Kroll, S. Bonhommeau, T. Kachel, H. A. Dürr, J. Werner, G. Behr, A. Koitzsch, R. Hübel, S. Leger, R. Schönfelder, A. K. Ariffin, R. Manzke, F. M. F. de Groot, J. Fink, H. Eschrig, B. Büchner, and M. Knupfer, *Phys. Rev. B* **78**, 220502 (2008).
- ⁴⁰ S. Raghu, X.-L. Qi, C.-X. Liu, D. J. Scalapino, and S.-C. Zhang, *Phys. Rev. B* **77**, 220503(R) (2008).
- ⁴¹ E. Z. Kurmaev, A. L. Ankudinov, J. J. Rehr, L. D. Finkelstein, P. F. Karimov, and A. Moewes, *J. Electr. Spectr. Rel. Phenom.* **148**, 1 (2005).
- ⁴² V. I. Anisimov, J. Zaanen, and O. K. Andersen, *Phys. Rev. B* **44**, 943 (1991).